

1
2
3
4
5
6
7
8
9
10
11
12
13
14
15

Supporting Information for
Abnormally shallow boundary layer associated with severe air
pollution during the COVID-19 lockdown in China

Tianning Su¹, Zhanqing Li¹, Youtong Zheng¹, Qingzu Luan^{2,1}, Jianping Guo³

¹Department of Atmospheric and Oceanic Sciences & ESSIC, University of
Maryland, College Park, Maryland 20740, USA

²Beijing municipal climate center, Beijing 100081, China

³State Key Laboratory of Severe Weather, Chinese Academy of Meteorological
Sciences, Beijing 100081, China

Correspondence to: zli@atmos.umd.edu

16 **1. Inverse fitting**

17 Since the PBLH and PM_{2.5} are correlated but not linearly correlated under most
18 conditions, the inverse function [$f(x) = A/x + B$] is used to fit the relationship.
19 Following Winship and Radbill (1994), the fitting parameters (A and B) and the
20 coefficient of determination of the PBLH–PM_{2.5} relationship are derived using this
21 inverse fitting function. The correlation coefficient of the inverse fit would be positive
22 when PBLH and PM_{2.5} are positively correlated, otherwise it would be negative.
23 Moreover, the normalized sample density at each location in a scatter plot represents the
24 probability distribution in two dimensions (Scott, 2015). Then setting the weighting
25 function of the inverse fit equal to the normalized density produces the best-fitting results
26 representing the majority of cases. The magnitude of the correlation coefficient (R^\dagger) is
27 designed to represent the degree to which the data fit an inverse relationship.

28

29 **2. Standardized multiple linear regression**

30 We use a standardized multiple linear regression method following previous
31 studies (Igel and van den Heever, 2015; Stolz et al., 2017). The confounding
32 relationships between daily PM_{2.5} and multiple meteorological factors are established by
33 the standardized regression equation. The standardized regression equation with seven
34 predictor variables x_1, x_2, x_3, x_4 (PBLH, WS, RH, and rainfall amount) and the response
35 y (PM_{2.5}) can be written as:

$$36 \quad y = \alpha_1 x_1 + \alpha_2 x_2 + \alpha_3 x_3 + \alpha_4 x_4 \quad (1)$$

37 where y and x_i are standardized variables derived from the raw variables Y and X_i by
38 subtracting the sample means (Y, X_i) and dividing by the sample standard deviations ($\delta_Y,$
39 δ_i):

$$40 \quad y = \frac{Y - \bar{Y}}{\delta_Y}, \quad x_i = \frac{X_i - \bar{X}_i}{\delta_i}, i = 1, 2, 3, 4 \quad (2)$$

41 Standardized regression coefficients ignore the independent variables' scale of units,
42 which makes the slope estimates comparable and shows the relative weights to the
43 changes in LSP occurrence hours. A partial correlation is done to control the other
44 predictors and to study the effect of each predictor separately.

45

46 **3. Similarity check**

47 For searching the similar meteorological condition of CLD haze event over Beijing,
48 we use the five-day smoothed time series of each parameter during winter from 2013
49 to 2020. For instance, we define the PBLH condition is similar, if the difference in
50 five-day smoothed time series is less than 20%, which means:

$$51 \quad |\overline{PBLH}_A - \overline{PBLH}_{CLD}| < 20\% \overline{PBLH}_{CLD} \quad (3)$$

52 where A is a five-day period, \overline{PBLH}_A and \overline{PBLH}_{CLD} represent the mean value of PBLH
53 during period A and CLD, respectively. The procedure is the same for WS and RH.
54 Moreover, we defined all three parameters are similar if the difference in five-day
55 smoothed time series is less than 20% for both PBLH, WS, and RH.

56

57 **References**

58 Stolz, D. C., Rutledge, S. A., Pierce, J. R., and van den Heever, S. C.: A global lightning
59 parameterization based on statistical relationships among environmental factors,
60 aerosols, and convective clouds in the TRMM climatology, *J. Geophys. Res.-*
61 *Atmos.*, 122, 7461–7492, <https://doi.org/10.1002/2016JD026220>, 2017.

62 Igel, M. R. and van den Heever, S. C.: The relative influence of environmental
63 characteristics on tropical deep convective morphology as observed by CloudSat,
64 *J. Geophys. Res.-Atmos.*, 120, 4304–4322, Winship, C. and Radbill, L.:
65 Sampling weights and regression analysis, *Sociol. Method. Res.*, 23, 230–257,
66 1994. <https://doi.org/10.1002/2014JD022690>, 2015.

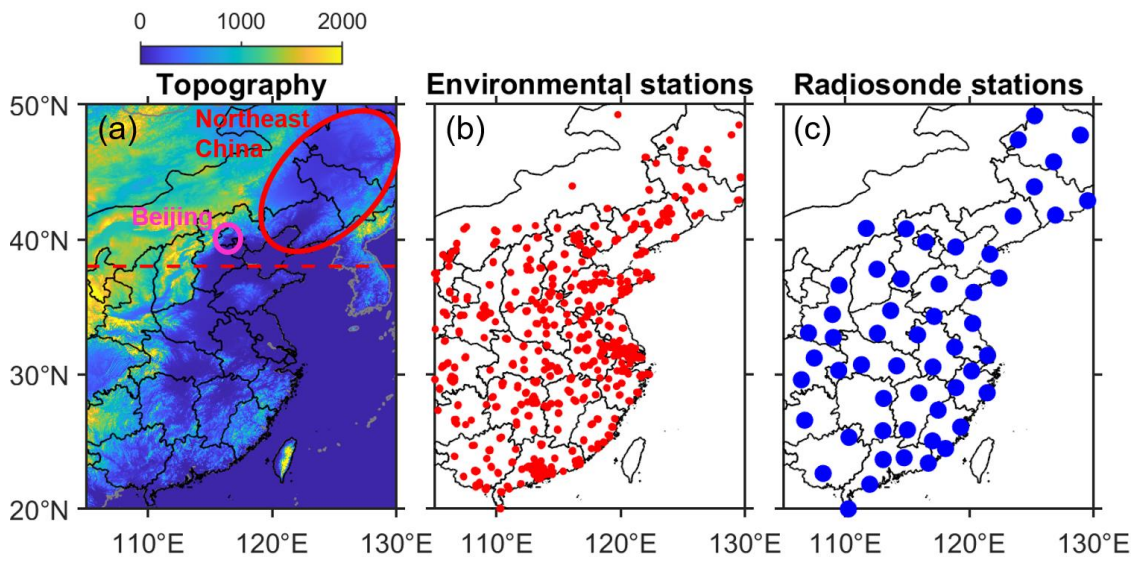
67 Winship, C. and Radbill, L.: Sampling weights and regression analysis, *Sociol. Method.*
68 *Res.*, 23, 230–257, 1994

69 Scott, D. W.: Multivariate density estimation: theory, practice, and visualization, John
70 Wiley & Sons, USA, 2015.

71

72

73 **Figures**



74

75 **Figure S1.** (a) Topography of eastern China. The red line divided northern China and
76 southern/central China. Beijing and Northeast China are highlighted by the pink circle
77 and red circle, respectively. (b) Locations of environmental monitoring stations. (c)
78 Locations of radiosonde stations.

79

80

81

82

83

84

85

86

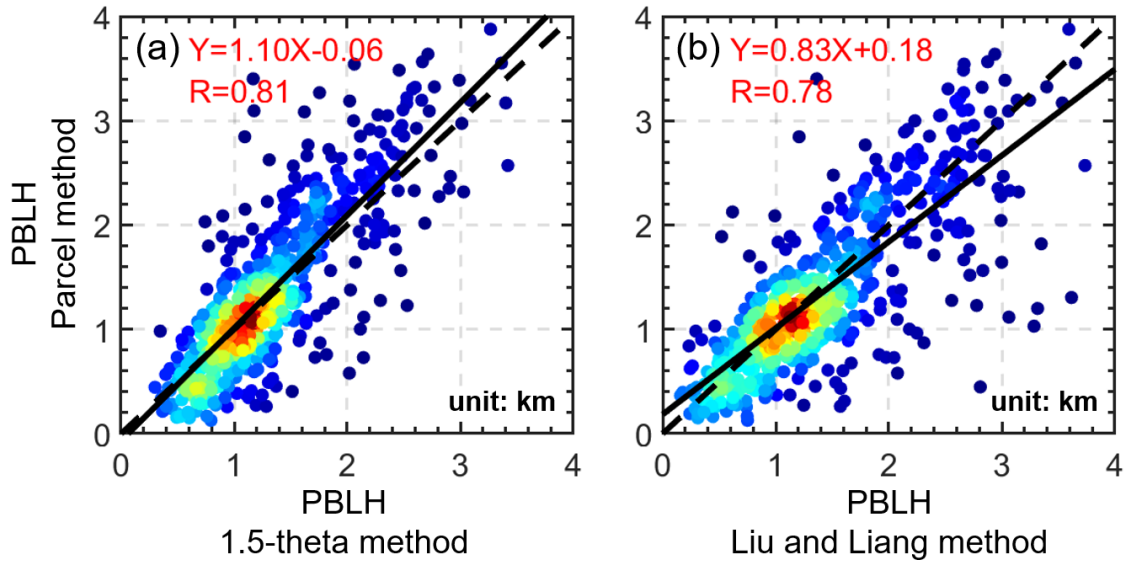
87

88

89

90

91



92

93 **Figure S2.** The comparison of PBLHs derived from parcel method and two standard
 94 methods (1.5-theta method and Liu and Liang method) at 1400 BJT during summertime.
 95 Parcel method uses morning radiosonde and surface meteorological data, and standard
 96 methods use radiosonde at 1400 BJT. The linear regression equations and correlation
 97 coefficients (R) are given in each panel.

98

99

100

101

102

103

104

105

106

107

108

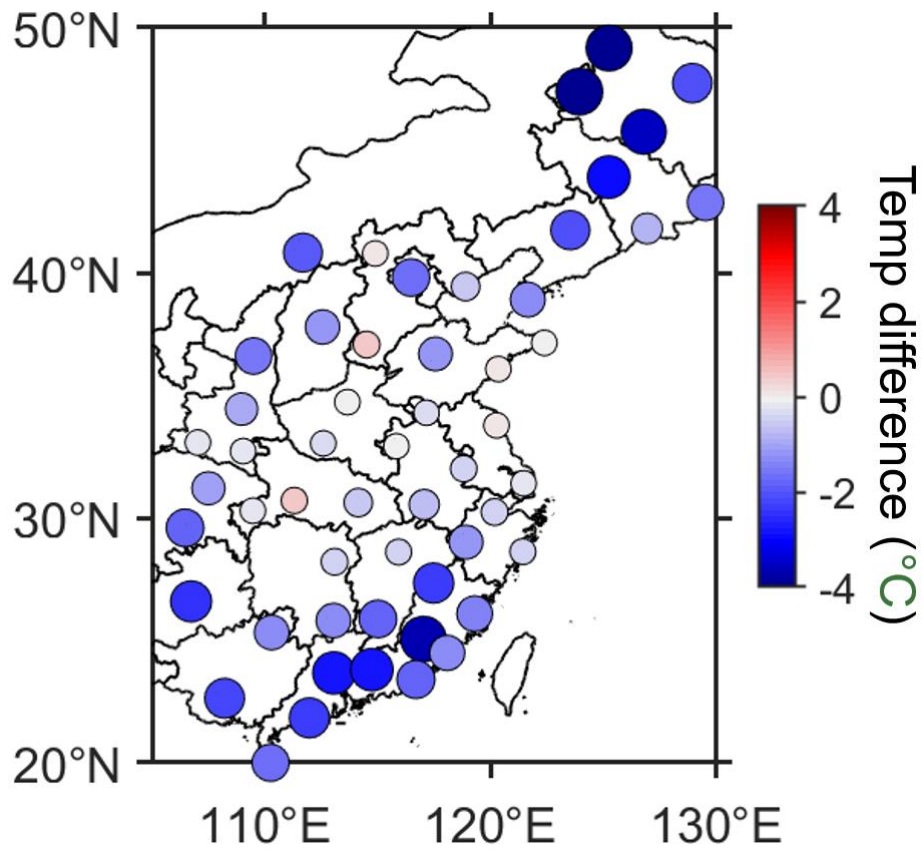
109

110

111

112

113



114

115 **Figure S3.** The differences in daytime temperature between mean values during the
116 COVID-19 lockdown and the climatological mean during the same period of the years
117 2016 to 2019.

118

119

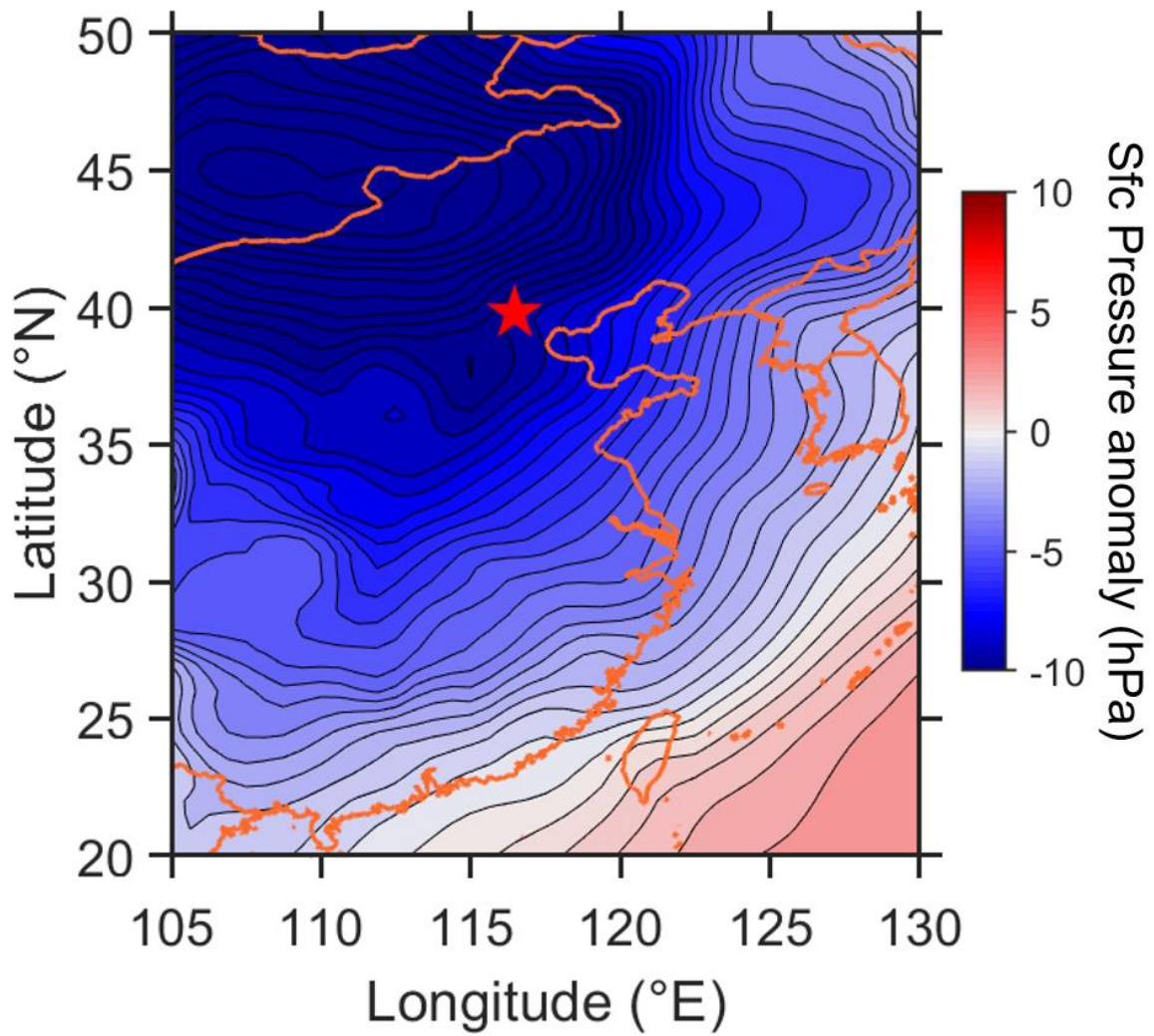
120

121

122

123

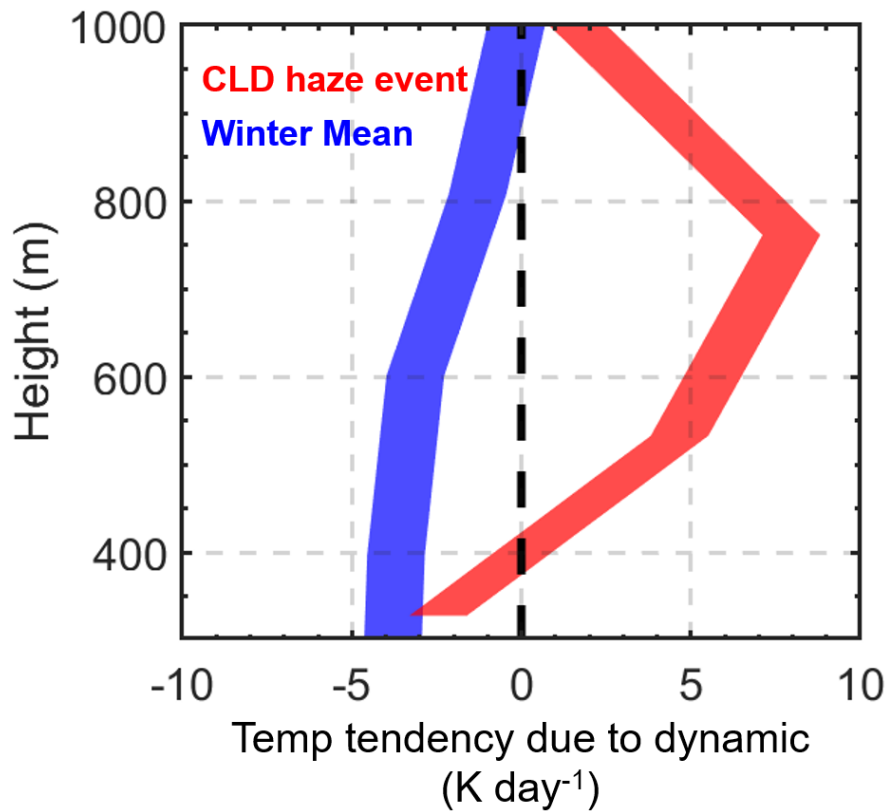
124



125

126 **Figure S4.** The surface pressure anomalies (relative to the monthly mean) during the
127 CLD haze event. The location of Beijing is marked as the red star. The orange line
128 indicates the coastline/border. The data are obtained from MERRA-2 reanalysis data.

129



130

131 **Figure S5.** Profiles of temperature tendency due to the dynamic processes from
 132 MERRA-2 reanalysis data. Red line represents the value at 1230 BJT during the CLD
 133 haze event, and blue line represents the corresponding mean value during winter. The
 134 structure of temperature tendency during the CLD haze event facilitate the temperature
 135 inversion, and thus increase the lower-atmosphere stability and reduce the PBLH.

136 **Tables**

137 **Table S1.** List of radiosonde stations over Beijing and northeast China.

138 (<http://data.cma.cn/en/>)

Regions of interest	Station code	City	Elevation (m)
Beijing	54511	Beijing	30
Northeast China	54662	Dalian	90
	50953	Harbin	143
	54161	Changchun	239
	50745	Qiqihar	148
	54292	Yanji	256

139

140

141

142

143

144

145

146

147

148

149

150

151

152

153

154

155

156

157

158

159

160

161 **Table S2.** Statistics of the partial correlation coefficients of the relationships between
 162 PM_{2.5} and multiple meteorological parameters (PBLH, WS, RH, and rainfall amount)
 163 during CLD. Also shown are standardized multiple regression equations of PM_{2.5} onto
 164 the meteorological parameters. Asterisks (*) denote the correlations that are statistically
 165 significant at the 95% confidence level. PBLH shows significant partial correlations with
 166 PM_{2.5} over both Beijing and Northeast China.

ROIs	Partial Correlation Coefficients with PM _{2.5} (y)			
	PBLH (x_1)	WS (x_2)	RH (x_3)	Rainfall (x_4)
Beijing	-0.50*	-0.05	0.18	-0.42*
	Standardized multiple regression: $y = -0.59x_1 - 0.05x_2 + 0.18x_3 - 0.45x_4$			
Northeast China	-0.44*	-0.41*	0.14	-0.19
	Standardized multiple regression: $y = -0.40x_1 - 0.41x_2 + 0.09x_3 - 0.13x_4$			

167
 168
 169
 170
 171
 172
 173
 174
 175
 176
 177
 178
 179
 180
 181
 182
 183
 184
 185
 186
 187

189 **Table S3.** PM_{2.5} and meteorology during CLD haze event and other three shallow PBL
 190 periods during 2013–2019.

	Date	PM _{2.5} (µg m ⁻³)	PBLH (m)	WS (m/s)	RH (%)
CLD haze event	20200213	212	425	2.3	84
	20200212	195	648	1.2	60
	20200211	232	437	1.6	60
	20200210	116	429	1.2	47
	20200209	127	507	1.6	58
Period I	20170104	287	237	1.3	78
	20170103	287	332	1.7	72
	20170102	231	133	2.3	67
	20170101	497	301	1.5	88
	20161231	312	545	1.4	70
	20161230	166	647	1.3	67
Period II	20161221	407	378	1.1	78
	20161220	362	241	1.3	89
	20161219	205	558	1.2	56
	20161218	213	512	1.1	61
	20161217	206	320	1.7	58
	20161216	108	522	1.2	47
Period III	20151226	239	245	1.9	79
	20151225	553	238	1.5	97
	20151224	58	296	1.5	74
	20151223	211	539	1.3	73
	20151222	306	168	1.9	86
	20151221	215	420	1.3	68